Research Article

Targeting Conformational Activation of CDK2 Kinase

Morgan Pellerano[1]*, Sergey Tcherniuk[1]*, Corine Perals[2]*, Thi Nhu Ngoc Van[1], Elsa Garcin[3], Florence Mahuteau-Betzer[4], Marie-Paule Teulade-Fichou[4], May C. Morris[1#]

[1]-Institut des Biomolécules Max Mousseron, CNRS UMR 5247, Université de Montpellier, Faculté de Pharmacie, Bât E, 15 Av. Charles Flahault, 34093 Montpellier, France

[2]- Centre de Physiopathologie de Toulouse Purpan, INSERM UMR 1043, CNRS UMR 5282, Université de Toulouse Paul Sabatier, CHU Purpan , BP3028, 31024 Toulouse Cedex 3, France

[3]-University of Maryland Baltimore County (UMBC), Department of Chemistry and Biochemistry, 1000 Hilltop Circle, Baltimore, MD 21250, USA

[4]-Institut Curie-CNRS UMR176, Bât. 110, Université Paris-Sud, F-91405 ORSAY, France

*these authors have contributed equally to the work

Correspondence: Dr. M.C. Morris, Institut des Biomolécules Max Mousseron, CNRS UMR 5247, Université de Montpellier, Faculté de Pharmacie, Bât E, 15 Av. Charles Flahault, 34093 Montpellier, France. **E-mail**: may.morris@umontpellier.fr

Keywords: allosteric regulation; cyclin-dependent kinase; fluorescent biosensor; high-throughput screening; inhibitor

Abbreviations:

CDK, Cyclin-dependent Kinase; **HTS**, High throughput screening

Please cite this article as doi: 10.1002/biot.201600531.

Submitted: 21-Sep-2016
Revised: 20-Apr-2017
Accepted: 21-Apr-2017

Abstract

Cyclin-dependent kinases constitute attractive pharmacological targets for cancer therapeutics, yet inhibitors in clinical trials target the ATP-binding pocket of the CDK and therefore suffer from limited selectivity and emergence of resistance. The more recent development of allosteric inhibitors targeting conformational plasticity of protein kinases offers promising perspectives for therapeutics. In particular tampering with T-loop dynamics of CDK2 kinase would provide a selective means of inhibiting this kinase, by preventing its conformational activation. To this aim we engineered a fluorescent biosensor that specifically reports on conformational changes of CDK2 activation loop and is insensitive to ATP or ATP-competitive inhibitors, which constitutes a highly sensitive probe for identification of selective T-loop modulators. This biosensor was successfully applied to screen a library of small chemical compounds leading to discovery of a family of quinacridine analogs, which potently inhibit cancer cell proliferation, and promote accumulation of cells in S phase and G2. These compounds bind CDK2/ Cyclin A, inhibit its kinase activity, compete with substrate binding, but not with ATP, and dock onto the T-loop of CDK2. The best compound also binds CDK4 and CDK4/Cyclin D1, but not CDK1. The strategy we describe opens new doors for the discovery of a new class of allosteric CDK inhibitors for cancer therapeutics.

1 Introduction

Physiological regulation of cell cycle progression is coordinated by a family of heterodimeric protein kinases, known as cyclin-dependent kinases [1, 2]. Biologically relevant CDK/cyclin complexes are formed through association of a CDK kinase subunit, which bears the catalytic function, with a regulatory cyclin partner which plays a major role in promoting activation of the CDK, in defining substrate specificity, and in targeting the heterodimeric complex to well-defined subcellular locations [3]. CDK activation is a complex process, which is initiated by the interaction with the cyclin subunit, and further proceeds through a series of regulatory phosphorylation/dephosphorylation steps [3-5].

Aside from their function in coordinating cell growth and division, cyclin-dependent kinases play a major role in sustaining cancer cell proliferation and thereby constitute attractive pharmacological targets [6]. In fact, CDK/Cyclins have served as targets for the identification of anticancer compounds from natural substances, for development of inhibitors by rational derivatization of ATP analogs, or by high-throughput screening of libraries of small molecules [6-10]. Strategies employed in drug discovery to screen for protein kinase inhibitors in general, and CDK/Cyclins in particular, rely on activity-based assays which have essentially lead to identification of ATP-competitive inhibitors [11, 12]. However most of these inhibitors display poor selectivity towards CDKs, which is not surprising given that the ATP-binding pocket of the 518 members of the human kinome is highly conserved and several other cellular enzymes also bind ATP. For this reason, alternative strategies have been devised, including tampering with catalytic activity by targeting the active site, interfering with substrate recognition, targeting protein/protein interactions involved in activation of these kinases, or competing with cyclin binding [13-17]. Recent work has revealed the potential and selectivity of allosteric inhibitors to target conformational transitions which are essential for protein kinase function. So far, however, very few allosteric inhibitors of cyclin-dependent kinases have been reported. A potential allosteric ligand binding site was described in a large pocket that extends from the DFG region above the C-helix of CDK2 [18], and a recent virtual screen lead to the identification of type III allosteric inhibitors that bind this pocket, with anti-proliferative activity in breast cancer cells in the micromolar range [19].

CDK2/cyclin A, the archetype of CDK/Cyclins, has been extensively characterized both from a structural and mechanistic point of view, revealing that cyclin A binding induces significant conformational changes in the CDK, namely rotation of the N-terminal lobe leading to alignment of the ATP-binding site with the catalytic cleft, required for efficient transfer of phosphate onto the substrate, and a positional switch of the activating segment, also known as the activation loop or T-loop, which becomes partially stabilized in a position enabling access to the substrate [20-23]. Subsequent phosphorylation of the T-loop by the CDK-Activating Kinase CAK further displaces the T-loop, thereby generating a fully accessible substrate-binding site, favouring substrate binding, and consequently contributing to full activation of the CDK/Cyclin complex [22, 24]. Tampering with T-loop dynamics would potentially provide a selective means of inhibiting CDK2, by preventing conformational activation of this kinase, as well as substrate binding. However, so far, no allosteric inhibitors targeting the activation loop of CDK2 have been reported. To this aim, we designed a fluorescent biosensor that reports on conformational changes of the T-loop by introducing fluorescent "molecular hinges" into the protein scaffold of CDK2. This biosensor was subsequently used in a high-throughput screen to identify novel selective inhibitors of CDK2 effective in preventing cancer cell proliferation, resulting in the discovery of a new class of inhibitors derived from quinacridines targeting the T-loop of CDK2.

2 Materials and methods

2.1. Chemical Compound Library used in the screen

A total of 18480 small molecule chemical compounds were obtained from four different French laboratories that participate in the French National Chemical Compound Library. Institut Curie, Orsay (Florence MAHUTEAU-BETZER/Marianne BOMBLED) – 8560 480 compounds ; Faculté de Pharmacie de Strasbourg, ILLKIRCH (Marcel HIBERT/Bruno DIDIER) – 5040 480 compounds ; Institut de Chimie des Substances Naturelles, Gif-sur-Yvette (Alain MONTAGNAC/Olivier PAMLARD) – 4400 compounds ;

Institut de Chimie Organique et Analytique, Orléans – 480 compounds (Luc MORIN ALLORY/ Laurent ROBIN).

2.2. Other reagents

Nocodazole etoposide, propidium iodide, RNAse A, Crystal violet and McCoy's 5A medium were purchased from Sigma. Cell culture media, serum and antibiotics were purchased from Life technologies. Monoclonal anti-γ-H2AX and polyclonal anti–phospho histone H3 were obtained from Upstate Biotechnology; anti-Pan-actin, anti-cleaved Caspase-9, anti-Caspase-3 and anti-poly ADP ribose polymerase (PARP) from Cell Signaling; anti-β-tubulin and anti-p53 from Sigma, anti-cyclin A, B1, D and E, anti-CDK1, CDK2, CDK4 and anti-p21 from Santa Cruz Biotechnology.FITC–conjugated donkey anti-mouse, anti-rabbit antibodies were from Jackson ImmunoResearch and goat anti-rabbit and anti-mouse HRP-conjugated antibodies from Promega.

2.3. Expression and purification of CDKs, Cyclins and CDK2 mutants

GST-CDK2, GST-CDK4, GST-CDK1, GST-Cyclin A, GST-Cyclin D1 and His-Cyclin A were expressed in *Escherichia coli* and purified as described previously [25]. The C118S, C177S, C191S, C118S/C177S and C118S/C191S mutants of CDK2 were expressed in *E. coli* as GST fusions by IPTG induction 3h at 37°C, then purified by affinity and size exclusion chromatography on GST-Trap and Superdex75 columns, respectively. CDKCONF biosensor was then obtained by purifying the C118S mutant and labelling it with tenfold molar excess fluorescein or Cy3 maleimide and further purified from free label on NAP-5 columns.

2.4. CDK2/Cyclin A Kinase Activity Assays

Recombinant CDK2/CyclinA was prepared as described previously [23] and its activity assayed in a standard phosphorylation assay using 50nM kinase, 3uM histone H1 (H4524 Sigma) and radioactive 33P-gamma-ATP, essentially as described previously [23, 14]. Curve fitting was performed using GraFit, Software, Erithacus Ltd [25] and IC50 was calculated using the "IC50 full 4 param" equation, in which "Range" is the fitted uninhibited value minus the background (i.e. residual activity), and s is the slope factor :

$$y = \frac{Range}{1+\left(\frac{x}{\mathrm{IC}_{50}}\right)^{s}} + \mathrm{Background}$$

2.5. Steady-State Fluorescence Experiments.

Fluorescence experiments were performed as described previously [25]. Fluorescent biosensor was diluted to 200 nM in 1ml buffer and titrated with increasing concentration of cofactor, cyclin partner, histone substrate or inhibitors, at 25°C, using a SPEX-PTI spectrofluorimeter in a 1 cm path-length quartz cuvette, with a band-pass of 2 nm for excitation and emission, respectively. Emission spectra were recorded between 500 and 540 nm following excitation at 495 nm, and between 560 and 600 nm following excitation at 550nm, for fluorescein and Cy3 labelled CDK2 mutants, respectively. For characterization of MMQ binding to CDKs and CDK/Cyclin complexes, MMQ emission spectra were recorded at 460 nm following excitation at 355 nm on a POLARstar BMG 96-well plate reader. Data were corrected and fitted as described previously, using a quadratic equation and the GraFit Software, Erithacus Ltd [25].

2. 6. Automated High throughput screening conditions and hit validation

Prior to the HTS, stability assays and downscaling experiments were performed to establish the best conditions for a miniaturized assay in 384-well plates and optimized so as to obtain a robust and reproducible signal. Performance criteria for reproducibility, sensitivity (in the presence of DMSO), tolerance and robustness were established with ATP and two ATP analogs, roscovitine and staurosporine, that barely affect CDKCONF fluorescence and the 5 μM C4 peptide, as a positive control, that promotes significant enhancement of CDKCONF. Optimal screening conditions were established as follows: 5nM freshly purified CDKCONF-Cy3 (3 days old max, stored at 4°C) was stabilized in 50

mM Tris-HCl pH 7.5, 150 mM NaCl, 1 mM EDTA and 10% glycerol, 1% DMSO, for 1 hour at room temperature in the dark. CDKCONF-Cy3 was first tested manually on 48 assays (controls including C4 peptide, roscovitine and staurosporine) before starting the run (an average of 20 384-well plates/day). Conditions achieved: fluorescence with the C4 peptide was amplified by 84% and the factor Z>=0.5 (mean, standard deviation).

The screen itself was performed in 384-well black Costar plates. Compounds from the library were used at 10^{-5} M final concentration against 5nM CDKCONF-Cy3 in Tris buffer, pH 7.2, 150 mM NaCl and fluorescence emission of Cy3 was measured at 579 nm following excitation at 550nm. The C4 peptide inhibitor[10] was used as a reference/positive intraplate control to measure changes in CDKCONF-Cy3 fluorescence throughout the screen at a final concentration of 5 μM. After 30 minutes of incubation in the dark at room temperature, Cy3 fluorescence was quantified with an Envision® plate reader (Perkin Elmer, USA) using an excitation filter at 531 nm (BODIPY TMR531, Perkin Elmer) and an emission filter at 579 nm (Emission 579, Perkin Elmer). In parallel, the intrinsic fluorescence of the library compounds at 579 nm following excitation at 531 nm was determined, to eliminate autofluorescent compounds. The increase in fluorescence was calculated with reference to the basal fluorescence of CDKCONF-Cy3 alone and is expressed as the percentage of increase. A molecule was considered a hit when it was not autofluorescent, yet induced amplification of CDKCONF-Cy3 fluorescence 3 times or greater the standard deviation of CDKCONF-fluorescence alone (or p=0.01).

Hits identified in the screen were retested manually in quadruplet to confirm they were positive hits with a fresh batch of CDKCONF-Cy3 and stock solutions of the library compounds in DMSO. Determination of the potency (EC50) of the hits (solid supplies) were performed with a range of 8 concentrations from from 2.25 μM to 225 μM. The results were analyzed with Graph Pad Prism® version 4.

2.7. Cell Lines and Cell Culture

All cell lines were purchased from ATCC, except for HCT116 p53(-/-)provided by Dr. D. Skoufias (IBS, Grenoble, France), MESSA Dx5 cells by Dr. L. Lafanechère (CNRS, UMR 5168/CEA/IRTSV, Grenoble, France), TS/A murine mammary adenocarcinoma cells by JL Coll (UJF, Grenoble) and MFH 148 by F. Chibon (IBCI, Bordeaux, France). All cell lines were cultured at 37°C in an atmosphere containing 5% CO_2. MESSA, MESSA Dx5 MDR, A549 and H358 cells were cultivated in the RPMI 1640 medium supplemented with 2 mM L-glutamine, 1% penicillin/streptomycin and 10% FBS. HCT116, HCT116 p53(-/-) and HT29 were cultivated in McCoy's 5A medium supplemented with 1% penicillin/streptomycin and 10% FBS. All other cell lines were grown in DMEM supplemented with 2 mM L-glutamine, 1% penicillin/streptomycin and 10% FBS.

2.8. Cell viability and cytotoxicity assays

Cell viability of A549 cells treated with different hit compounds was determined by luminescence using the ATPlite 1st Step Perkin Elmer ® assay. In this assay, ATP consumption (marker of cell viability) is determined as relative to the production of light caused by the reaction of ATP with added Dluciferin/luciferase. Luminescence was monitored with an Envision® plate reader.

For all other cell types, cell viability was determined by Crystal violet assay as the percentage of live cells compared to the control, in duplicate and in three independent experiments [26]. 96–well plates were seeded with 4-5x10^3 cells/well and cells were incubated with inhibitor compounds for 72-96 h. At the desired time point the medium was removed and cells were washed with PBS and fixed with formaldehyde (4%) for 10 minutes at room temperature. Then cells were stained with crystal violet (0.1 %) for 30 minutes at room temperature. After three washes in the distilled water the plates were dried and crystal violet was solubilized in acetic acid (10%) for 40 min. Absorbance of solubilized crystal violet was measured at 595 nm. Cell viability was calculated as the percentage of live cells compared to the control. The viability assay was performed in duplicate in three independent experiments. The statistical significance of the difference between the control and treated groups was determined by t-criterion of Student. P-value ≤ 0.05 was considered to be statistically significant.

2.9. Flow cytometry

Cells at 40-50 % of confluence were treated with inhibitor compounds for 24, 48, 72h. All cells, including both attached and non-attached cells, were stained with propidium iodide and analysed by flow cytometry by FACScan (Becton Dickinson flow cytometer), using the CellQuest software. For each sample 10 000 events were collected and aggregated cells were gated out.

2. 10. Immunofluorescence

Cells cultured to 50-60 % confluence on poly-D-lysine–coated coverslips were treated with drugs and then fixed with 2% paraformaldehyde in PBS for 20 min at 37°C, permeabilized with 0.2% Triton in PBS for 5 min at room temperature, and processed for immunofluorescence with anti-β-tubulin and anti-γ-H2AX Abs diluted 1:400 and 1:100, respectively, in PBS containing 3% BSA, 0.05% Tween and 0.02% sodium azide, then incubated with FITC-conjugated secondary antibodies at 1:250 dilution for 30 min at 37°C. Cells were counterstained with propidium iodide at 0.5 μg/ml, washed in PBS three times for 5 min, and mounted on microscopic slides with Mowiol. Images were captured with a Zeiss AxioimagerZ1 motorized microscope, restored by the deconvolution programme Huygens Remote Manager (HMR) and analyzed using the Metamorph software.

2.11. Docking of MMQ3 onto CDK2 and CDK2/Cyclin A.

To perform the docking studies, we used the docking webserver SWISSDOCK (Web Server issue: W270-7, Grosdidier, A., Zoete, V. , Michielen, O.). First, we defined the protein structure as either CDK2 alone (PDBcode 1B38) or the complex CDK2/cyclin A (PDBcode 1fin), and the ligand structure as MMQ3. The PRODRG server [27] was used to convert the ligand file into MOL2 format, required for SWISSDOCK. We used default parameters for « accurate docking » as provided by the SWISSDOCK server. The docking result contained 18 clusters with 8 docking poses for each cluster. We manually examined each pose in PYMOL Molecular Graphics System, Version 1.1.

3 Results

3.1. Design and characterization of CDKCONF – a conformation-sensitive sensor of CDK2. CDK2 bears three cysteine residues within the C-terminal lobe that constitute attractive candidates for sensing molecules that bind near and/or affect the conformation of the T-loop. C118 is located on alpha helix E, which lies close to, yet not in direct contact with, the activation loop of CDK2. C177 is located at the tip of the T-loop, in close proximity to T160 and Y179, which contacts Cyclin A. C191 is located on alpha helix F, which immediately follows the T-loop, and is in close contact with T-loop residues W167 and Y168 **(Fig. 1A).** To generate a sensor reporting on conformational changes of the T-loop associated with CDK2 activation, we took advantage of these cysteine groups, which we labelled individually, and in pairs with the synthetic fluorophore, fluorescein to assess their ability to report on Cyclin A-induced conformational changes. This study revealed that C177- and C191-labelled CDK2 (C118S/C191S and C118S/C177S mutants), and to a greater extent the dual-labeled C177/C191 CDK2 (C118S mutant), serve as sensitive reporters of CDK2 C-lobe isomerization (**Fig. 1, B and C; Table S1**). The C177- C191- FITC-labelled C118S mutant of CDK2 was further characterized *in vitro* to determine its sensitivity and specificity in response to known cofactors, inhibitors and histone H1 substrate (**Fig. 1, C and D; Table S1**). These experiments revealed that ATP/ ADP addition resulted in modest changes in fluorescence of C177/C191-labelled-CDK2. Likewise, fluorescence emission was not significantly affected upon titration with the ATP-pocket kinase inhibitor roscovitine (**Fig. 1C**) or with histone H1 substrate (**Fig. 1D**). In contrast, titration with the C4 peptide, which binds a cleft at the interface between CDK2 and Cyclin A and close to the T-loop [14], induced a 10-fold increase in fluorescence at saturation (**Fig. 1C**). These data indicate that C177/C191-labelled CDK2 is sensitive to biomolecules that bind near the T-loop and affect its conformation, but not to compounds that bind in the ATP-binding pocket or the substrate-binding cleft, and therefore constitutes an ideal reporter of CDK2 isomerization and activation, which we termed CDKCONF.

3.2. Application of CDKCONF to a high throughput screen and identification of hit compounds. Given the preferential response of CDKCONF to biomolecules that bind the T-loop of CDK2, we used it to identify allosteric inhibitors affecting the positional switch of this loop associated with kinase activation. CDKCONF was tested to screen a library of 18,480 small molecule chemical compounds obtained from the French National Chemical Compound Library (ICSN, ICOA, Institut Curie, Illkirch). To this aim, CDKCONF was labeled with Cy3, which yields a more stable signal than fluorescein over time. A flowchart of the screen is presented in **Fig. 2A**, and experimental details described in the Experimental Procedures section. A total of 264 compounds out of the 18480 (1.43%) lead to significant enhancement of CDKCONF-Cy3 fluorescence. 201 of these (1.1% of the library) were autofluorescent and were therefore excluded from further testing. The 63 remaining compounds (0.34% of the library) were retested individually and 47 (0.25% of the library) were retained based on their ability to promote fluorescence enhancement of CDKCONF-Cy3 to at least the same extent or greater than the C4 reference peptide (**Table S2**). Further characterization of these compounds revealed very different mechanisms of action. Only nine compounds promoted a concentration-dependent increase in CDKCONF-Cy3 fluorescence and were selected for further testing (**Table S3**). Four compounds induced greater than 200% amplification of fluorescence at 100 μM (**Fig. 2B:** LPS 20-26-L-H02, ICC103-L018-D11, ICC008-L110-D08, ICC154-L148-G09). Five compounds promoted maximal enhancement of fluorescence between 125 and 200% at 100 μM (**Fig. 2C:** LPS 02-26-L-G09, ICC008-L143-C07, ICC154-L148-G06, ICC154-L148-H04, ICC154-L148-H05). The remaining compounds did not exhibit any dose-dependency (**Fig. 2D)**.

3.3. Characterization of hits on cell proliferation and cell cycle progression. The inhibitory potential of these nine compounds was first assessed in proliferation assays using different cancer cell lines. Proliferation assays with A549 cells revealed that seven of these compounds inhibited cell proliferation with IC50 values ranging from 0.1 μM to 1 μM (**Fig. 3A, Table S4).** Based on this assay, the four compounds presenting the greatest anti-proliferative activity were retained as leads for the rest of the study. These compounds feature a meta-quinacridine scaffold and were hereafter termed MMQ3 (ICC154-L-148-G06), MMQ12 (ICC154-L-148-G09), MMQ8 (ICC154-L-148-H04) and MMQ9 (ICC154-L-148-H05) [28]. The structures of these compounds are shown in **Fig. 3B** and their physical properties regarded as indicators of Lipinski's rules of "drug-likeness" are summarized in **Table 2**. All of these compounds have molecular masses somewhat above 500 Da (between 500-600 if the chlorine groups are excluded). However all compounds are characterized by an octanol-water partition coefficient (log P) below 5 and no more than 10 hydrogen bond acceptors. MMQ3,8 and 9 do not present more than 5 hydrogen bond donors, and therefore comply with 3 out of the 4 Lipinski's rules.

The efficacy of these leads to inhibit cell proliferation and perturb cell cycle progression was further characterized in the HeLa, MESSA and MESSA Dx5 cell lines. MMQ3, MMQ8, and MMQ9 were efficient inhibitors of HeLa cell proliferation compared to MMQ12 and roscovitine (**Table 1; Fig. S1A)**. Moreover, the cell cycle distribution profiles of HeLa cells treated with these compounds for 48 h revealed that MMQ3 and MMQ8, and to a lesser extent MMQ9, had a noticeable effect on cell cycle progression, promoting an overall accumulation of cells in S phase and in G2 (**Fig. 3C)**. Similar experiments were performed on the MESSA cell line and its drug-resistant counterpart MESSA Dx5 (that expresses an active PgP efflux pump [29]. These experiments revealed a similar hierarchy in anti-proliferative efficacies of the different compounds, the most potent being MMQ3 and MMQ8, although they were 6-12 fold less potent in MESSA cells than in HeLa cells (**Table 1; Fig. S1B)**. They also revealed significant differences between MESSA and MESSA Dx5 cells, which allowed us to determine the relative resistance towards these compounds. Like roscovitine, the relative resistance of multidrug-resistant (MESSA Dx5) compared to non-resistant MESSA cells for MMQ3, MMQ9 and MMQ12 was fairly low, emphasizing the importance of these compounds for chemotherapy of drug-resistant cancers. Further analysis of the cell cycle distribution profiles of MESSA and MESSA Dx5 cells treated with these drugs for 72h revealed that MMQ3 and 9 had the most significant effect, whilst MMQ8 had a visible effect on MESSA Dx5, but not on MESSA cells (**Fig. 3D)**. Since these data indicated that MMQ3 was the most potent inhibitor with the lowest EC50 values, we further determined its anti-proliferative activity in a large panel of different cell lines, including breast, lung, prostate and colon

cancer (**Table 3**). In all of these cell types, IC50 values were in the submicromolar range, from 30±3 nM for MFH 148 to 416±35 nM for MESSA and 812±53 nM for the MESSA Dx5 multi-drug resistant cell line. We also found that MMQ3 was also a potent inhibitor of cancer cell lines of murine origin, including mouse melanoma B16, glioblastoma GL26 and mammary adenocarcinoma TS/A cell lines. Based on these data, MMQ3 was retained as the main lead and further characterized to gain insight into its mechanism of action.

3.4. MMQ3 promotes accumulation of cells in S phase and G2 and induces apoptosis. Treatment of unsynchronized HeLa cells with MMQ3 promoted dose-dependent and time-dependent decline in the levels of cyclins A, D, and E, whilst this effect was not observed with either roscovitine or etoposide (**Fig. 4A)**. Likewise, phosphorylation of CDK1 at residue Y15, of histone H3 and of Rb at residue S780 disappeared in a dose- and time-dependent fashion, whereas cyclin D1 , CDK1, CDK2, p21 and p53 levels remained unchanged. Cyclin A and E are required for DNA synthesis and progression through S phase, associated with CDK2 activity during S phase, whilst Cyclin A is further involved in progression through G2 and entry into mitosis, its levels dropping in pro-metaphase [30]. Cyclin B1 begins to accumulate in G2 phase and reaches peak levels in metaphase, after which it is subject to degradation by ubiquitin-mediated proteolysis [31]. Whilst CDK2 is the main kinase responsible for progression through S phase and G2, CDK1 kinase is held in check during G2 through phosphorylation of Y15 by Wee1 kinase and is then activated through dephosphorylation by Cdc25 phosphatases [32-34]. The observation that histone H3 and CDK1 phosphorylation at residue Y15 decrease upon treatment with MMQ3 infers that cells are accumulating prior to mitosis. Moreover the observed decline in cyclin A, E and B levels associated with higher concentrations of MMQ3 suggests that these cyclins no longer form stable complexes with CDK2, thereby clearly preventing CDK2 from performing its cellular functions, since this requires cyclin binding. Interestingly we observed an accumulation of phosphor (S780) in cells treated with 1.25 and 2.5 uM MMQ3 after 12h treatment, suggesting that CDK4 is targeted by MMQ3 at this early stage [35]. However, this phosphorylation disappears at later time points, indicating that cells are no longer accumulating in G1. Taken together these data suggest that cells treated with MMQ3 progress beyond G1, and accumulate in S and G2, in line with the FACS experiments.

To further assess the fate of cells treated with MMQ3, we asked whether apoptosis was induced. Western Blotting analysis of HeLa cells treated with 2.5 μM MMQ3 reveals dose- and time-dependent accumulation of cleaved poly (ADP-ribose) PARP-1, caspase 3 and capase 9 (**Fig. 4B)**. Likewise, prolonged treatment (48-72h) with lower concentrations of MMQ3 (0.6-1.25 μM) induced apoptosis. In agreement with these observations, flow cytometry profiles revealed the appearance of sub-G1 peak corresponding to an apoptotic population. Time-lapse videomicroscopy further revealed that HeLa cells treated with MMQ3 arrested rapidly with a rounded morphology, at a stage prior mitosis and remained rounded up for 24 hours prior to apoptosis (data not shown).

3.5. Mechanism of Action of MMQ3. Compounds MMQ3-12 are penta-heterocyclic structures with slight differences on their polyamino chains, known as quinacridine derivatives, which were previously characterized as specific binders of DNA quadruplex structures and inhibitors of telomerase *in vitro* [36, 37]. However since the primary target of MMQs in cells was never identified, and treatment with MMQ3 leads to accumulation of HeLa cells in S and G2 phases, we asked whether it might behave as a DNA-damaging agent, through intercalation and/or by inducing breaks in double-stranded DNA. To this aim, we compared the effect of MMQ3 with that of etoposide, a well characterized inhibitor of topoisomerase II, that promotes accumulation of DNA strand breaks [38]. Whereas treatment with etoposide lead to clear appearance of DNA strand breaks, associated with phosphorylation of H2AX histone, MMQ3 did not result in any detectable appearance of γ-H2AX foci, indicating that this compound is not a classical DNA-damaging agent (**Fig. 5A**). We also asked whether MMQ3 might exert its effect by perturbing microtubule integrity in interphase or on mitotic spindle assembly in metaphase, like other well characterized cancer drugs, such as nocodazole [39], but did not observe any detectable effect (**Fig. S2**).

In order to verify that the MMQ3 indeed inhibited CDK2 activity directly, we characterized its ability to inhibit kinase activity of recombinant CDK2/Cyclin A kinase in a radioactive kinase assay using histone H1 as a substrate (**Fig. 5B)**. This experiment revealed that MMQ3 indeed inhibited CDK2/Cyclin A activity *in vitro*, with an EC50 value of 25 μM. Moreover, CDK2/CycA kinase activity was only partially inhibited by MMQ3, with a maximum of 60% inhibition at the highest concentrations of enzyme tested (200 μM). This might reflect the allosteric behaviour of MMQ3 which may interfere with the conformational transition of the kinase to its active form, thereby maintaining it in an intermediate conformation which is catalytically less efficient yet still capable of phosphotransfer activity.

To gain further insight into the mechanism of action of MMQ3, we characterized its ability to bind CDK2 and Cyclin A directly. To this aim, we took advantage of the intrinsic fluorescent properties of MMQ3**,** and monitored changes in its fluorescence upon incubation with CDK2, Cyclin A or the CDK2/Cyclin A complex (**Fig. 5C)**. Although MMQs were initially isolated as binders of a monomeric CDK2 derivative (CDKCONF-Cy3) these experiments revealed that the intrinsic fluorescence of MMQ3 was not significantly affected upon titration with CDK2, inferring that its overall environment was very similar in solution and when binding CDK2. Likewise no change in fluorescence was observed upon titration with Cyclin A. In contrast, MMQ3 fluorescence underwent a strong quenching upon addition of increasing concentrations of the CDK2/Cyclin A complex**,** inferring that it binds in a very different environment in the CDK2/Cyclin A complex as compared to that of CDK2 protein alone, and fitting of the fluorescence titration curve yielded a dissociation constant of 28nM **(Fig. 5C)**. Similar results were found for MMQ8, 9 and 12, with dissociation constants of 114nM ±64 nM, 125nM ±35 nM and 174nM ±26 nM respectively **(Fig. S3A)**. We further addressed whether MMQ3 might also bind other CDKs by monitoring changes in the intrinsic fluorescence of MMQ3, upon titration with CDK1, CDK4 or CDK4/Cyclin D. As observed for CDK2, MMQ3 fluorescence was not significantly affected upon titration with CDK1. In contrast, titration with both CDK4 and CDK4/CyclinD led to significant fluorescence enhancement of MMQ3, with dissociation constant values of 0.82 ±0.55 nM and 3.95 ±2 nM, respectively, indicating that both monomeric and cyclin D-complexed CDK4 constitute targets of MMQ3 **(Fig. 5D)**. However compared to the fluorescence quenching of MMQ3 observed upon titration with CDK2/Cyclin A, this fluorescence enhancement infers that MMQ3 binds a very different environment and possibly mode in CDK2 and CDK4.

Finally, we asked whether MMQ3 binding to the CDK2/Cyclin A complex might prevent or compete with substrate binding. To this aim, we performed displacement experiments using histone H1, the classical substrate used in radioactive-based kinase assays. Whereas binding of MMQ3 to CDK2/Cyclin A promoted significant quenching of its fluorescence, addition of histone H1 reverted this quenching, suggesting that histone H1 can displace MMQ3 from CDK2/Cyclin A. In contrast, addition of increasing concentrations of ATP did not promote any changes in the fluorescence of MMQ3 complexed to CDK2/Cyclin A, inferring that ATP binding does not interfere or compete with MMQ3 (**Fig. 5E).** Similar results were found for MMQ9, the second best hit, whereas MMQ8 and 12 binding to CDK2/Cyclin A was displaced by ATP, but not by histone H1, inferring a different binding mode and mechanism of action **(Fig. S3B).**

3.6. Identification of MMQ3 binding site on CDK2. To identify the potential binding site(s) of MMQ3 on CDK2, we performed a docking study (**Fig. 6**). We used the webserver SWISSDOCK to dock MMQ3 to either CDK2 alone or to the CDK2/Cyclin A complex. Manual inspection of the clustered docking poses to the complex allowed us to exclude poses that were located primarily next to Cyclin A (cluster 4), poses that were too far from the T-loop to be significant (clusters 1-3, 5-8, 10-12, 14, 17, and 18), and poses located in the ATP binding site.

These results are summarized in **Table S5** and **Fig. S4**. The most promising poses (cluster 9) are located within 3 Å of T-loop residues L148, T158, T160, V163, and within 3.5 Å of CDK2 core residues D127, I173, G176, C177, P234, D235, and E208 (**Fig. 6A-C and Table S5**). Interestingly, E208 is involved in the interaction of CDK2 with CksHs1 [40], a small structural regulator of CDK2/CyclinA which is essential for regulation of its activation through recruitment of phosphoprotein regulators to

CDK2 [41]. Moreover MMQ3 lies in close contact with the regulatory phosphorylation sites T14 and Y15 [3-5].

To experimentally validate the binding site of MMQ3 suggested by the docking experiment, we used the CDKCONF-Cy3 mutants C118S/C191S and C118S/C177S. These Cy3-labelled mutants were compared to CDKCONF-Cy3 in fluorescence titration experiments with MMQ3, revealing that the C118S/C177S mutant did not undergo any significant changes in fluorescence upon titration with MMQ3, in contrast to the C118S/C191S mutant (**Fig. 6*D***). These results indicate that C177 is involved in a direct interaction with MMQ3, consistent with the docking results. Moreover, calculation of the dissociation constant based on the titration curve of the C118S/C191S mutant, yielded a value of 1.5 nM, indicating that MMQ3 binds very tightly to Cy3-labelled C177-CDK2. Further studies are in progress to try and determine the exact binding site of MMQ3 to CDK2 via X-ray crystallography.

4 Discussion

Cyclin-dependent kinases and their regulators constitute established biomarkers, as well as attractive pharmacological targets for the development of anticancer drugs. Studies providing insights into the molecular mechanisms of CDK/cyclin activation have provided clues for the structure-guided design of novel classes of inhibitors, targeting essential protein/protein interfaces and/or residues required for structural organization. However to date drug discovery programs have essentially yielded compounds that target the ATP-binding pocket of CDKs, since screening strategies have relied on activity-based assays. Although some of these compounds have successfully made it to clinical trials, they tend to suffer from a lack of selectivity, due to the high conservation of the ATP-binding pocket throughout the 518 kinases in the human genome.

In an effort to improve selectivity, more recent approaches have focused on the design of inhibitors that bind less conserved sites outside the ATP pocket, compounds that bind inactive kinase conformations and allosteric inhibitors that target a conformational transition which is essential for kinase activation [42-45]. These classes of inhibitors are considered potentially more selective, since they bind to residues within sites that are not conserved amongst kinases, and can therefore serve as a basis to develop potent anticancer inhibitors. However, it has proven extremely difficult to identify allosteric inhibitors in high throughput screening assays, due to a general lack of selective strategies to discriminate such compounds from classical active site binders. As such, only two families of allosteric inhibitors of cyclin-dependent kinases have been described so far: a family of cyclin-competitive CDK2 type II inhibitors that target the DFG in/out transition [17] and type III inhibitors that bind an allosteric pocket between the DFG loop and the C helix of CDK2 [19].

Protein conformational switches are ubiquitous in nature and often regulate key biological processes. The vast majority of protein enzymes can switch conformation upon specific stimulation or trigger mechanisms, including post-translational modification, cofactor binding or association with a regulatory partner [46]. Proteins can switch between distinct folded, disordered and aggregation states, and protein kinase activity is regulated through conformational plasticity and dynamic reorganization of the activation segment conformation [47, 48]. Binding of Cyclin A to CDK2 plays a central role in the activation of CDK2 by promoting major structural rearrangements that enable ATP binding and provide substrate access to the catalytic cleft, in particular a major conformational change of the activation segment, or T-loop. Indeed, the T-loop behaves like a drawbridge in preventing substrate binding to the monomeric form of the kinase, but swings open upon binding of the cyclin to the CDK. The conformational changes of the T-loop therefore constitute an attractive target for inhibitors of CDK/Cyclin activity.

In this study we describe an original protein-based conformation-sensitive fluorescent biosensor based on the scaffold of CDK2 kinase, that can report on conformational changes of the T-loop associated activation of CDK2. Specifically, two fluorescent cyanine dyes introduced at specific positions within the scaffold of a CDK2 mutant, serve as molecular hinges that sense conformational changes of the T-loop. Moreover this biosensor is essentially insensitive to ATP-pocket ligands, thereby constituting a sensitive probe to screen for allosteric inhibitors targeting T-loop dynamics,

whilst discriminating ATP-competitive inhibitors of CDK2. We have provided a proof-of-concept of the applicability of this biosensor by screening 18480 chemical compounds from the French National Compound Library in a high-throughput format and successfully identifying a novel class of CDK2 inhibitors, a family of structural analogs with pentacyclic quinacridine scaffold known as MMQs. These compounds constitute potent inhibitors of a wide variety of cancer cell lines with IC50 values in the submicromolar range. Moreover multidrug-resistant (MESSA Dx5) exhibit a fairly low relative resistance to these compounds (MMQ3, 9 and 12], in the same range as the ATP-competitive CDK inhibitor roscovitine, emphasizing their potential for chemotherapy of drug-resistant cancers.

MMQs were previously characterized as binders of DNA quadruplex structures and inhibitors of telomerase in vitro [36, 37]. Interestingly DNA G-quadruplex structures have recently been visualized in human cells and shown to be modulated during cell cycle progression [49]. Hence it is possible that the cellular phenotype we observe upon treatment of cancer cells with MMQs is at least in part associated with their ability to bind DNA quadruplex structures. However, we have clearly shown in this study that MMQs interact directly with recombinant CDK2/Cyclin A complex with high affinity (Kd values between 28 and 174nM] and inhibit its kinase activity with an EC50 value of 25uM. In line with these experiments, treatment of cells with MMQ3 led to accumulation of cells in S phase and G2, associated with a decline of cyclin A, E and B levels, inferring a destabilization of CDK2/Cyclin complexes and consequent degradation of cyclins. Cyclin D levels in contrast were not affected, indicating that cells passed the restriction point, although MMQ3 treatment did promote accumulation of phosphoRb after 12h treatment, suggesting that CDK4/Cyclin D1 may constitute an early target. In agreement with this observation, we found that MMQ3 indeed interacted with recombinant CDK4 and CDK4/Cyclin D1.

The lead compound identified in our screen, MMQ3 inhibits CDK2 kinase activity by preventing substrate binding (histone) but not ATP, inferring it prevents a conformational transition required for substrate access and binding. Moreover, docking studies reveal that MMQ3 binds across the T-loop of CDK2 and interacts with several residues within the CDK core that line the T-loop, including C177 and E208, a residue involved in binding to the small structural regulator CksHs1; it could further make contacts with phosphorylation site residues T14 and Y15. Consistently, site-directed mutagenesis revealed that Cys177 was particularly sensitive to MMQ3 binding. Although the exact binding mode of MMQ3 may only be determined via structural studies, our docking and fluorescence results suggest a general binding pocket near the T-loop and the CDK2-Cyclin A interface, which constitutes an attractive targeting interface for new generations of allosteric CDK2 inhibitors.

CDKCONF biosensor constitutes a useful and sensitive tool for screening complex libraries of synthetic compounds to identify modulators and potential allosteric inhibitors that tamper with the T-loop conformational switch. Moreover, it constitutes a potent chemical biology tool for studying the mechanism of activation and inhibition of cyclin-dependent kinases from a fundamental perspective. In fact, the concept we describe in this manuscript, based on a fluorescent protein-biosensor which allows to identify modulators of protein kinase conformation, is more generally applicable to probe cofactors, regulatory partners, substrates and inhibitors that induce conformational changes in the kinase fold.

Acknowledgements
This work was supported by the CNRS (Centre National de la Recherche Scientifique) and grants from the CNRS (PEPs, exploratory project) and the Region Languedoc-Roussillon (Subvention “Chercheuse d’Avenir”) to MCM. TNNV was recipient of a fellowship from the USTH. ST was funded by a grant from INCA. We acknowledge all of the laboratories who have contributed to this study by making their compounds available through the French National Chemical Library: Institut de Chimie des Substances Naturelles , Gif-sur-Yvette, Faculté de Strasbourg, UMR7175-LC1 CNRS-ULP, Institut Curie, UMR176, Orsay and Institut de Chimie Organique et Analytique, UMR6005, Orléans. We thank Gilles Divita and Frederic Ausseil, USR3388 CNRS Pierre Fabre, for fruitful discussions and support to this project.

Conflict of interest

The authors declare no financial or commercial conflict of interest.

5 References

[1] Malumbres, M., Barbacid, M., Mammalian cyclin-dependent kinases. *Trends Biochem Sci.* 2005, *30*, 630-641.

[2] Malumbres, M., Physiological relevance of cell cycle kinases. *Physiol. Rev.* 2011*, 91,*973-1007

[3] Morgan, D.O., Cyclin-dependent kinases: Engines, Clocks, and Microprocessors. *Annu Rev Cell Dev Biol.* 1997*, 13*, 261-291

[4] Obaya, A.J., Sedivy, J.M., Regulation of cyclin-Cdk activity in mammalian cells. *Cell. Mol. Life Sci.* 2002, *59*, 126-142

[5] Satyanarayana, A., Kaldis, P., Mammalian cell-cycle regulation : several Cdks, numerous cyclins and diverse compensatory mechanisms. *Oncogene* 2009, *28*, 2925-2939

[6] Lapenna, S., Giordano, A., Cell cycle kinases as therapeutic targets for cancer. *Nat. Rev. Drug Discovery* 2009, *8,* 547-566

[7] Malumbres, M., Barbacid, M., Cell cycle, CDKs and cancer: a changing paradigm. *Nat.Rev.Cancer* 2009, *9*,153-166

[8] Noble, M., et al., Exploiting structural principles to design cyclin-dependent kinase inhibitors. *Biochim Biophys Acta.* 2005, *1754*, 58-64

[9] De Azevedo, W.F. , et al., Inhibition of cyclin-dependent kinases by purine analogues: crystal structure of human cdk2 complexed with roscovitine. *Eur. J. Biochem.* 1997, *243,* 518-526

[10] Vassilev, L.T., et al., Selective small-molecule inhibitor reveals critical mitotic functions of human CDK1. *Proc. Natl. Acad. Sci. USA.* 2006, *103,* 10660-10665

[11] Huwe, A., Mazitschek, R., Giannis, A., Small Molecules as Inhibitors of Cyclin-dependent Kinases. *Angew.Chem.Int.Ed.* 2003, *42*, 2122-2138

[12] Gray, N.S. , et al., Exploiting chemical libraries, structure and genomics in search for kinase inhibitors*. Science,* 1998, *281*, 533-538

[13] Mendoza, N., et al., Selective Cyclin-dependent kinase 2/Cyclin A antagonists that differ from ATP site inhibitors block tumor growth. *Cancer Research* 2003, 63, 1020-1024

[14] Gondeau, C., et al., Design of a novel class of peptide inhibitors of cyclin-dependent kinase/cyclin activation. *J. Biol.Chem.* 2005, *280*, 13793-13800

[15] Canela, N., et al., Identification of an Hexapeptide that binds to a surface pocket in cyclin A and inhibits the catalytic activity of the complex cyclin-dependent kinase 2-cyclin A. *J.Biol. Chem.* 2006, *281*, 35942- 35953

[16] Giordano, A. , Ballacchio, E. ,Bagella, L. , Paggi, M.G., Interaction between the Cdk2/Cyclin A complex and a small molecule derived from the pRb2/p130 spacer domain. *Cell Cycle* 2007, *6,* 2591-93

[17] Alexander, L.T., Möbitz H, Drueckes P, Savitsky P, et al., Type II inhibitors targeting CDK2. *ACS Chem. Biol.* 2015, *10*, 2116-25

[18] Betzi, S., Alam R., Martin M., Lubbers DJ, et al., Discovery of a potential allosteric ligand binding site in CDK2. *ACS Chem. Biol.* 2011*, 6*, 492-501.

[19] Rastelli G, Anighoro A, Chripkova M, Carrassa L, Broggini M., Structure-based discovery of the first allosteric inhibitors of cyclin-dependent kinase 2. *Cell Cycle* 2014, *13*, 2296-305.

[20] De Bondt, H.L. , et al., Crystal structure of cyclin-dependent kinase 2. *Nature* 1993, *363,* 595-602

[21] Jeffrey, P.D., et al., Mechanism of CDK activation revealed by the structure of a cyclinA-CDK2 complex. *Nature* 1995, *376*, 313-320

[22] Russo, A.A., et al., Structural basis of cyclin-dependent kinase activation by phosphorylation. *Nat. Struct. Biol.* 1996, *3*, 696-700

[23] Morris, M.C., Gondeau, C., Tainer, J.A., Divita G., Kinetic Mechanism of Activation of the Cdk2/Cyclin A complex. *J. Biol.Chem.* 2002, *277*, 23847-53

[24] Brown, N.R. , et al., Effects of phosphorylation of threonine 160 on cyclin-dependent kinase 2 structure and activity. *J. Biol.Chem.,* 1999, *274*, 8746-56

[25] Heitz, F., et al., Interactions of cyclins with cyclin-dependent kinases: a common interactive mechanism. *Biochemistry* 1997, *36*, 4995-5003

[26] Gillies, R.J.,,Didier, N., Denton, M., Determination of cell number in monolayer cultures. *Anal Biochem.* 1986, *159*,109-113

[27] Schüttelkopf, A.W., van Aalten, D.M.F., Acta Crystallogr. 2004, *D60*: 1355

[28] Baudoin, O. , Teulade-Fichou, M.P., Vigneron, J.P., Lehn, J.M., Cyclobisintercaland macrocycles : synthesis and physicochemical properties of macrocyclic polyamines containing two crescent-shaped dibenzophenanthroline subunits. *J.Org. Chem.* 1997, *62*, 5458

[29] Harker, W.G., Sikic, B.I., Multidrug resistance in Doxorubicin-selected Variants of the Human Sarcoma Cell Line MES-SA. *Cancer Res.* 1985, *45*, 4091-4096

[30] Pagano, M., Pepperkok, R., Verde, F., Ansorge, W., Draetta, G., Cyclin A is required at two points in the human cell cycle. *EMBO J.* 1992, *11*, 961-971

[31] Clute P., Pines J., Temporal and spatial control of cyclin B1 destruction in metaphase. *Nat.Cell.Biol.* 1992, *1*, 82-87

[32] Atherton-Fessler, S. , et al., Cell cycle regulation of the p34cdc2 inhibitory kinases. *Mol. Biol. Cell.* 1994, *5*, 989-1001

[33] McGowan, C.H. , Russell, P., Human Wee1 kinase inhibits cell division by phosphorylating p34cdc2 exclusively on Tyr15. *EMBO J.* 1993, *12*, 75-85

[34] Honda, R., et al., Dephosphorylation of human p34cdc2 kinase on both Thr-14 and Tyr-15 by human cdc25B phosphatase. *FEBS Lett.* 1993, *318*, 331-334

[35] Lundberg, A.S., Weinberg R.A. Functional inactivation of the retinoblastoma protein requires sequential modification by at least two distinct cyclin-cdk complexes. *Mol. Cell Biol.* 1998, *18,* 753-761

[36] Honsou, C., et al., G-quadruplex recognition by quinacridines : a SAR, NMR, and biological study. *ChemMedChem.* 2007, *2*, 655-666

[37] Mergny, J.L. , et al., Telomerase inhibitors based on quadruplex ligands selected by a fluorescence assay. *Proc Natl.Acad Sci.* 2001, *98*, 3062-67

[38] Ross, W., et al., Role of topoisomerase II in mediating epipodophyllotoxin-induced DNA cleavage. *Cancer Res.* 1984, *44*, 5857-60

[39] Tcherniuk, S., et al., UA62784 is a cytotoxic inhibitor of microtubules, not CENP-E. *Chem.Biol.* 2011, *18*, 631-641

[40] Bourne, Y., et al., Crystal structure and mutational analysis of the human CDK2 kinase complex with cell cycle regulatory protein CksHs1. *Cell* 1996, *84*, 863-874

[41] Patra, D., Wang, S.X., Kumagai, A., Dunphy, W.G., The xenopus Suc1/Cks protein promotes phosphorylation of G(2)/M regulators. *J Biol Chem.* 1999, *274*, 36839-42

[42] Liu, Y., Gray N.S., Rational design of inhibitors that bind to inactive kinase conformations. *Nat. Chem. Biol.* 2006, *2*, 358-364

[43] Eglen, R.M., Reisine, T., Human kinome drug discovery and the emerging importance of atypical allosteric inhibitors. *Expert Opin Drug Discov.* 2010, *5*, 277-290

[44] Eglen, R., Reisine, T., Drug discovery and the human kinome: recent trends. *Pharmacol Ther.* 2011, *130*, 144-156

[45] Fang, Z., Grutter, C., Rauh, D., Strategies for the selective regulation of kinases with allosteric modulators: exploiting exclusive structural features. *ACS Chem.Biol.* 2013, *8*, 58-70

[46] Ambroggio, X.I., Kuhlman, B., Design of protein conformational switches. *Curr.Opin.Struct.Biol.* 2006, *16, 525-530*

[47] Nolen, B., Taylor, S., Ghosh, G., Regulation of Protein Kinases: controlling activity through activation segment conformation. *Mol. Cell.* 2004, *15*, 661-675

[48] Huse, M., Kuriyan, J., The conformational plasticity of protein kinases, *Cell* 2002, *109*, 275-282

[49] Biffi G, Tannahill D, McCafferty J, Balasubramanian S., Quantitative visualization of DNA G-quadruplex structures in human cells. *Nat Chem.* 2013, *5*, 182-6.

Table 1. IC50 of MMQ3, 8, 9, 12 on HeLa, MESSA and MESSADx5 cells

Compound	IC50 (nM) HeLa	IC50 (nM) MESSA	IC50 (nM) MESSA Dx5	Relative resistance*
MMQ3	70 ± 6	416 ± 52	812 ± 105	1.95
MMQ12	15000 ± 500	34111 ± 3158	22442 ± 4234	0.66
MMQ8	280 ± 15	1850 ± 663	61000 ± 4354	32.97
MMQ9	50 ± 8	354 ± 63	2348 ± 621	6.63
Roscovitine	4050±100	9500 ± 1940	5400 ± 952	0.57

*Relative resistance between the drug-resistant and parental MESSA cell lines.

Table 2 – Compliance of MMQ3,12,8 and 9 to Lipinski's Rules

Compound Name	Formula	Molecular weight	Log P	H bond acceptors	H bond donors	Lipinski's rule of 5
MMQ3	C32H46Cl6N6	727,46, or 517 without Cl	4,31	6	2	YES (3/4)
MMQ12	C34H56Cl8N10	888,49 or 608 without Cl	1,01	10	6	NO
MMQ8	C32H32Cl2N8	599,56 or 527 without Cl	4,00	6	4	YES (3/4)
MMQ9	C36H49Cl5N6O2	775,08, or 600 without Cl	3,88	8	2	YES (3/4)

Table 3. IC50 MMQ3 determined in different cell lines

Cell Line	IC50 (nM)
MFH 148	30± 3
LNcaP	47± 5
C 4-2	47± 4
A 375 m2	57,3± 6
A 375 p	59± 8
MDA MB 231	69.4± 4
HeLa	70± 5
DU 145	85± 7
HCT 116	90± 6
Eahy 926	102.4± 8
MFH 152	104.2± 11
IMR 90	115± 9
SW 620	120± 13
PC 3	130± 11
GL 26	130.2± 10
LoVo	146± 18
RPE-1	160± 14
H358	163.2± 13
H2OS	170± 12
KB 3-1	174± 14
B 16	200± 9
SW 480	215.3± 16
A 549	222.2± 13
H 1299	231± 19
HCT 116 p53-/-	280± 22
MCF 7	300± 30
MESSA	416± 35
TSA	460± 26
MESSA Dx5	812± 53

Figure legends

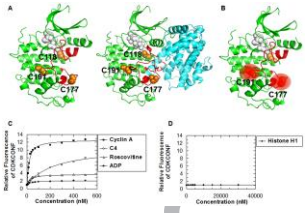

Figure 1. Design and characterization of CDKCONF (A) Structural representation of CDK2 (PDBcode: 1B38) and CDK2/CyclinA (PDBcode:1FIN) with the three naturally-occurring cysteine residues of CDK2: C118, C177 and C191 in orange. ATP is shown in white; CDK2 in green; the T-loop in red; cyclin A in cyan **(B)** The CDKCONF biosensor is obtained by labelling the CDK2 C118S mutant with an environmentally-sensitive fluorescent probe on residues C177 and C191 **(C)** Fluorescence titration of CDKCONF-fluorescein with ADP, the ATP-binding pocket inhibitor roscovitine, cyclin A, the C4 peptide and **(D)** histone H1.

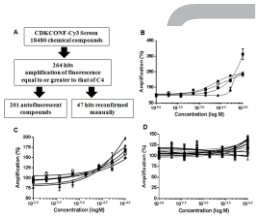

Figure 2. CDKCONF Screen and characterization of the fluorescence enhancement induced by hits (A) Flowchart of the screen performed with CDKCONF-Cy3. A library of 18,480 chemical compounds was screened and 264 hits were identified based on amplification of CDKCONF-Cy3 fluorescence equal to or greater than C4. 47 hits were reconfirmed independently and their ability to amplify CDKCONF-Cy3 fluorescence was determined as a function of their concentration. Results are represented with a non-linear regression fit designed with Graph Pad Prism ® version 4. **(B)** Compounds that induce greater than 200% amplification of fluorescence at 100 µM **(C)** compounds that promote between 125 and 200% fluorescence enhancement at 100 µM **(D)** examples of compounds that do not exhibit significant dose-dependent amplification of CDKCONF-Cy3 fluorescence.

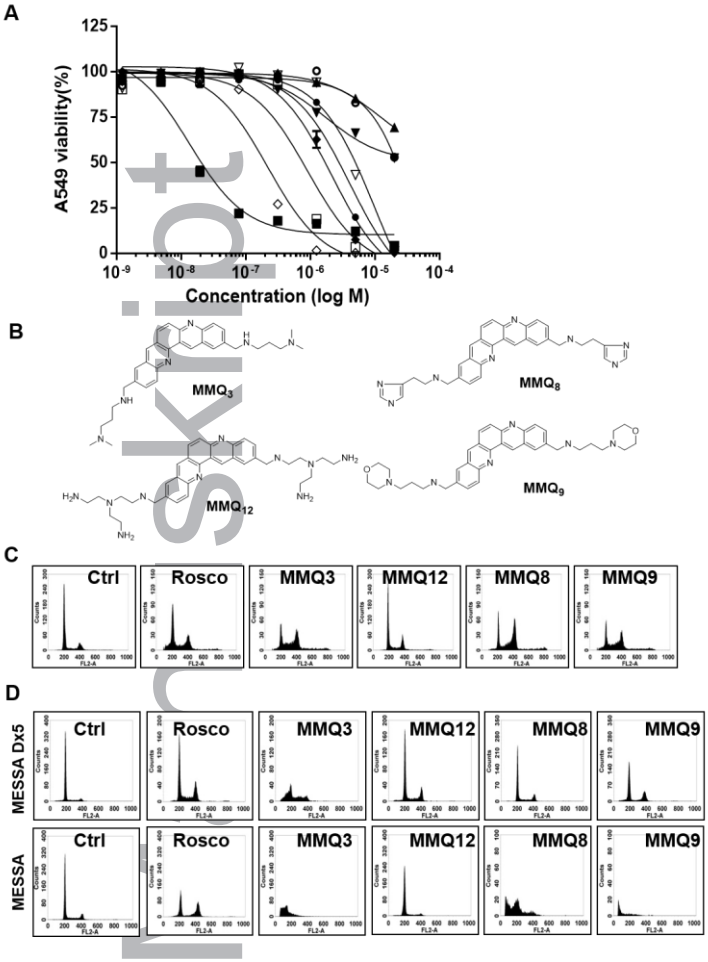

Figure 3. Characterization of hits on cell proliferation and cell cycle progression (A) Cytotoxicity of the best hits on A549 cells- percentage of cell viability is plotted against concentration. Black squares: nocodazole; black triangles pointing upwards: LPS 20-26-L-H02 ; black triangles pointing downwards: ICC008-L110-D08; black losanges : ICC103-L018-D11; black circles: ICC008-L143-C07; open squares: ICC154-L148-G06; open circles: ICC154-L148-G09; open triangles pointing down: ICC154-L148-H04. **(B)** Structural representation of the four lead compounds : MMQ3 : Meta-quinacridine (2-dimethylamino)ethylamine ; MMQ12 : Meta-quinacridine (N,N-bis(2-aminoethyl)ethylamine ; MMQ8 : Meta-quinacridine (3-(imidazol-1-yl))propylamine ; MMQ9 : Meta-quinacridine (3-(morpholin-1-yl))propylamine **(C)** Unsynchronized HeLa cells were treated with MMQ3, 8, 9, 12 or roscovitine for 48h and the cell distribution of cells in different cell cycle stages was assessed by flow cytometry. **(D)** Unsynchronized MESSA and MESSA Dx5 cells were treated with MMQ3, 8, 9, 12 or roscovitine for 48h for 72h and the distribution of cells in different cell cycle stages was assessed by flow cytometry.

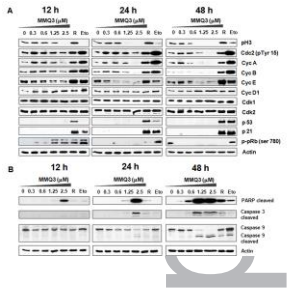

Figure 4. MMQ3 perturbs cell cycle progression and promotes apoptosis HeLa cells were treated with different concentrations of MMQ3 for 12, 24, and 48 h, roscovitine (8 μM) or etoposide (5 μM). Normalized cell extracts were subjected to SDS-PAGE and Western blotting **(A)** to assess the levels of different cell cycle regulators and markers : Cdk1, Cdk2, pTyr15-Cdk1: Cdk1 phosphorylated on tyrosine 15, Cyclin A, Cyclin B, Cyclin E, Cyclin D1, pH3: phosphohistone H3, p53, p21, pSer780-Rb: Rb phosphorylated on serine 780 **(B)** to determine the level of apoptotic markers : cleaved PARP, cleaved caspase-3 and cleaved caspase-9. Actin was used as a loading control.

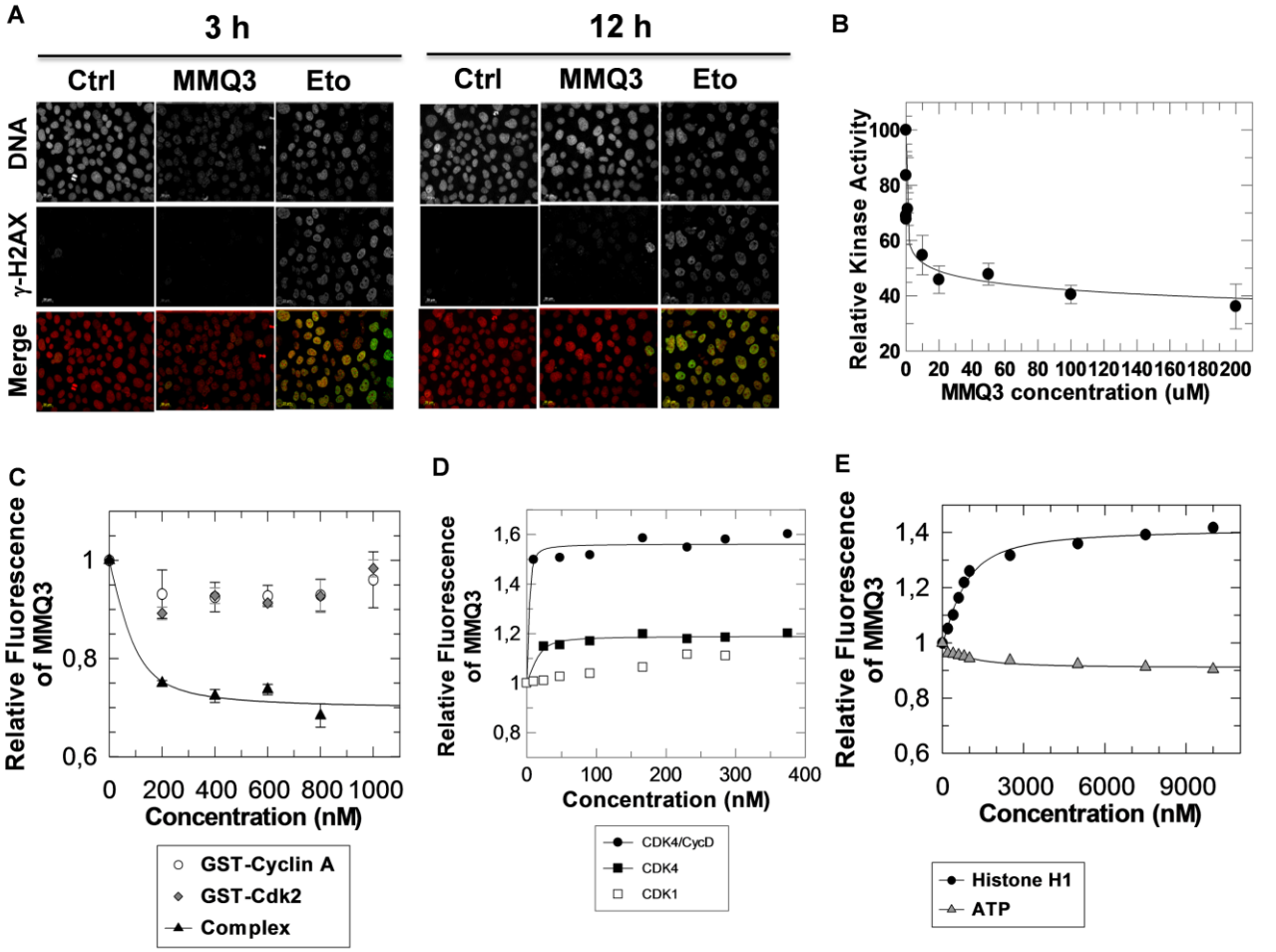

Figure 5. Mechanism of action of MMQ3

(A) HeLa cells were treated with MMQ3 (2.5 μM) or Etoposide (5 μM) for 3 -12 h. Histone γ-H2AX staining reveals the presence of DNA double-strand breaks in cells treated with etoposide, not with MMQ3. **(B)** Inhibition of recombinant CDK2/Cyclin A kinase activity by MMQ3 in a radioactive assay using histone H1 as a substrate. **(C)** MMQ3 docks preferentially onto CDK2/Cyclin A. The intrinsic fluorescence of 1μM MMQ3 (at 460 nm following excitation at 355 nm) was monitored following incubation with increasing concentrations of CDK2, Cyclin A or CDK2/Cyclin A. **(D)** MMQ3 titration with CDK1, CDK4 and CDK4/Cyclin D1. **(E)** MMQ3 binding to CDK2/Cyclin A is displaced by histone H1, not ATP. 1μM CDK2/Cyclin A complex was preincubated with 1μM MMQ3 (as shown in 5C), and its fluorescence was monitored upon titration with histone H1 or ATP.

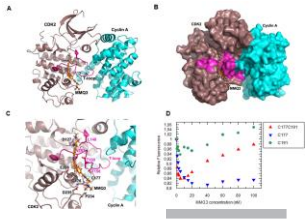

Figure 6. Docking of MMQ3 onto CDK2/Cyclin A (A) Docking of MMQ3 on the CDK2/Cyclin A complex: the most promising pose (cluster 9) is represented in sticks on the CDK2/Cyclin A X-ray structure (PDBcode 1fin), with CDK2 in salmon, T-loop in magenta, and Cyclin A in cyan. **(B)** The surface representation of the CDK2/Cyclin A complex with MMQ3 shows the binding pocket for MMQ3 near the T-loop and the CDK2/Cyclin A interface.**(C)** MMQ3 and the T-loop region – highlighting residues within 3.5 Å of MMQ3 (stick representation). **(D)** Fluorescence titration of CDKCONF-Cy3 (Cys177/Cys191- labelled CDK2) and of two Cys to Ser mutants, which only bear a single labelled cysteine, Cys177 or Cys191, with MMQ3.